



Obrabotka metallov -

Metal Working and Material Science

Journal homepage: http://journals.nstu.ru/obrabotka_metallov



Features of structure formation processes in AA2024 alloy joints formed by the friction stir welding with bobbin tool

Alexey Ivanov^{1, 2, a, *}, Valery Rubtsov^{1, 2, b}, Andrey Chumaevskii^{1, c}, Kseniya Osipovich^{1, d},
 Evgeny Kolubaev^{1, 2, e}, Vladimir Bakshaev^{3, f}, Ivan Ivashkin^{3, g}

¹ Institute of Strength Physics and Materials Science of Siberian Branch of Russian Academy of Sciences, 2/4 pr. Akademicheskii, Tomsk, 634055, Russian Federation

² Novosibirsk State Technical University, 20 Prospekt K. Marksa, Novosibirsk, 630073, Russian Federation

³ SESPEL Cheboksary enterprise, CJSC, 36 Leningradskaya st., Cheboksary, 428021, Chuvash Republic, Russian Federation

^a  <https://orcid.org/0000-0001-8959-8499>,  ivan@ispms.ru, ^b  <https://orcid.org/0000-0003-0348-1869>,  rvy@ispms.ru,

^c  <https://orcid.org/0000-0002-1983-4385>,  tch7av@gmail.com, ^d  <https://orcid.org/0000-0001-9534-775X>,  osipovich_k@ispms.tsc.ru,

^e  <https://orcid.org/0000-0001-7288-3656>,  eak@ispms.ru, ^f  <https://orcid.org/0000-0001-9777-0164>,  bakshaeva@mail.ru,

^g  <https://orcid.org/0000-0001-8808-2183>,  ivashkin_in@mail.ru

ARTICLE INFO

Article history:

Received: 15 March 2021

Revised: 25 March 2021

Accepted: 07 April 2021

Available online: 15 June 2021

Keywords:

Friction stir welding

Bobbin tool

Structure formation

Aluminum alloy

Funding

This work was performed within the frame of integrated project « Building of manufacturing of high-tech large-sized equipment for intelligent adaptive friction stir welding for aerospace and transport industries of the Russian Federation» (grant agreement from 22.11.2019 № 075-11-2019-033), implemented by SESPEL Cheboksary enterprise, CJSC, NETI and ISPMS SB RAS with the financial support of the Ministry of Education and Science of Russia in the context of Russian Government decree from 09.04.2010 № 218.

ABSTRACT

Introduction. One of friction stir welding types is the *bobbin friction stir welding* (BFSW) process, which allows to obtain welded joints in various configurations without using a substrate and axial embedding force, as well as to reduce heat loss and temperature gradient across the welded material thickness. This makes the BFSW process effective for welding aluminum alloys, which properties are determined by their structural-phase state. According to research data, the temperature and strain rate of the welded material have some value intervals in which strong defect-free joints are formed. At the same time, much less attention has been paid to the mechanisms of structure formation in the BFSW process. Therefore, to solve the problem of obtaining defect-free and strong welded joints by BFSW, an extended understanding of the basic mechanisms of structure formation in the welding process is required. **The aim of this work** is to research the mechanisms of structure formation in welded joint of AA2024 alloy obtained by bobbin tool friction stir welding with variation of the welding speed. **Results and discussion.** Weld formation conditions during BFSW process are determined by heat input into a welded material, its fragmentation and plastic flow around the welding tool, which depend on the ratio of tool rotation speed and tool travel speed. Mechanisms of joint formation are based on a combination of equally important processes of adhesive interaction in “tool-material” system and extrusion of metal into the region behind the welding tool. Combined with heat dissipation conditions and the configuration of the “tool-material” system, this leads to material extrusion from a welded joint and its decompaction. This results in formation of extended defects. Increasing in tool travel speed reduce the specific heat input, but in case of extended joints welding an amount of heat released in joint increases because of specific heat removal conditions. As a result, the conditions of adhesion interaction and extrusion processes change, which leads either to the growth of existing defects or to the formation of new ones. Taking into account the complexity of mechanisms of structure formation in joint obtained by BFSW, an obtaining of defect-free joints implies a necessary usage of various nondestructive testing methods in combination with an adaptive control of technological parameters directly in course of a welding process.

For citation: Ivanov A.N., Rubtsov V.E., Chumaevskii A.V., Osipovich K.S., Kolubaev E.A., Bakshaev V.A., Ivashkin I.N. Features of structure formation processes in AA2024 alloy joints formed by the friction stir welding with bobbin tool. *Obrabotka metallov (tehnologiya, oborudovanie, instrumenty) = Metal Working and Material Science*, 2021, vol. 23, no. 2, pp. 98–115. DOI: 10.17212/1994-6309-2021-23.2-98-115. (In Russian).

* Corresponding author

Ivanov Alexey N., Ph.D. (Engineering), Scientific associate
 Institute of Strength Physics and Materials,
 Science of Siberian Branch of Russian Academy of Sciences,
 2/4 pr. Akademicheskii,
 634055, Tomsk, Russian Federation
 Tel.: 8 (382) 228–68–63, e-mail: ivan@ispms.tsc.ru

Introduction

Conventional friction stir welding (CFSW) was developed to produce permanent joints of aluminum-based alloys with limited weldability. Among the FSW types, there is the bobbin tool welding (BFSW), which provides synchronous impact on the front and back surfaces of the material to be welded. It enables the production of welded joints of various configurations without the use of a substrate and reduces the rigidity of the welding equipment due to the absence of the axial penetration force typical for the conventional FSW [1, 2]. The BFSW is also characterized by reduced heat losses and temperature gradient across the thickness of the welded material [3, 4]. In comparison with CFSW, it provides homogenization of the welded joint structure, reduction of internal stresses and the property gradient in its main characteristic zones. In work [5] it is shown that during the CFSW and BFSW of AA6061 alloy, properties of produced joints are comparable with each other, but the BFSW process has a more limited range of admissible parameters. When comparing the CFSW and BFSW of AA6005 alloy [6], it was found that with the same process parameters, the BFSW process allows producing stronger joints. The authors of the works believed that these effects were caused by the above-mentioned features of temperature effect during the BFSW, which determines the kinetics of structure formation processes in the welded joint.

These features make the BFSW process effective for welding heat-treated aluminum alloys. In the work [7], during the BFSW of AA2198 alloy, the authors produced welded joints with an ultimate tensile strength of 82% compared to the initial alloy. The welding of joints made of AA7085 alloy [8] also resulted in tensile strength of more than 80% from the initial alloy. In this regard, the most interesting is the BFSW process of AA2024 alloy, the properties of which are determined by its structural-phase state. In its turn, it is closely connected with the thermomechanical influence [9, 10], therefore the final characteristics of AA2024 welded joints are highly dependent on welding process parameters [11, 12]. When considering the BFSW process, the parameters determining the properties of welded joints are the speed of welding and tool rotation, the depth of tool penetration, as well as the shape of the shoulder and pin [13–17]. According to the research data, the temperature and strain rate of the welded material caused by those parameters have some value ranges, in which strong defect-free joints are formed. At the same time, much less attention is paid to the mechanisms of structure formation in the BFSW process. To date, there are several works that simulate the mechanism of layer-by-layer transfer of the welded material during the BFSW [18, 19]. However, an extended understanding of the basic mechanisms of structure formation during the welding process is required to solve the problem of forming defect-free and strong welded joints by the BFSW process.

Consequently, the purpose of this work is to study the mechanisms of structure formation in the welded joint of AA2024 alloy at different welding speeds during the friction stir welding with a bobbin tool.

Methods

The research was carried out together with CJSC “Cheboksary Enterprise “SespeI”, using the original equipment and tools of in-house design for the friction stir welding. Welded joints were produced by the BFSW (Fig. 1, *a, b*) of AA2024 rolled sheets with the size of 100×250 mm and a thickness of 20 mm. Parameters of the tool are shown in Fig. 1, *c*. The chemical composition of AA2024 alloy is given in Table 1.

The welding was carried out as follows: the welding tool rotating with the frequency $\omega = 250$ rpm was introduced into the butt of the welded sheets from the end surface. At the introduction of the tool, its travel speed V was equal to 5 mm/min. Further, after the tool movement at the distance of 15 mm, the travel speed was increasing in each 5 mm up to values 7.5, 10, 15, 20, 25, 30, 35, 40 mm/min. The welding process was performed at the tool travel speed of 40 mm/min, while the tool rotation speed remained constant.

The research was carried out on specimens made using a DK7750 wire-EDM machine by cutting the welded joints according to the diagram in Fig. 2. The structure of the welded joint at its initial/outgoing sections was investigated (IN/OUT in Fig. 2). Longitudinal sections in the central region of the joint (CTR

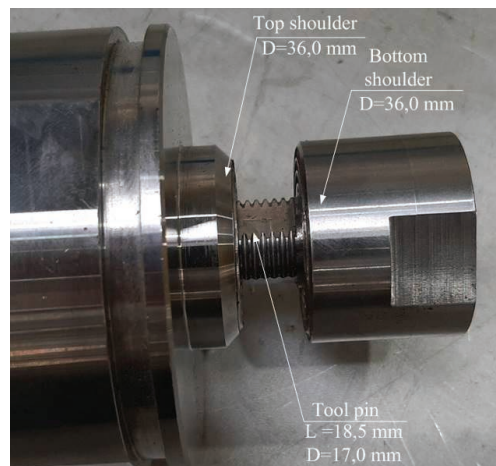
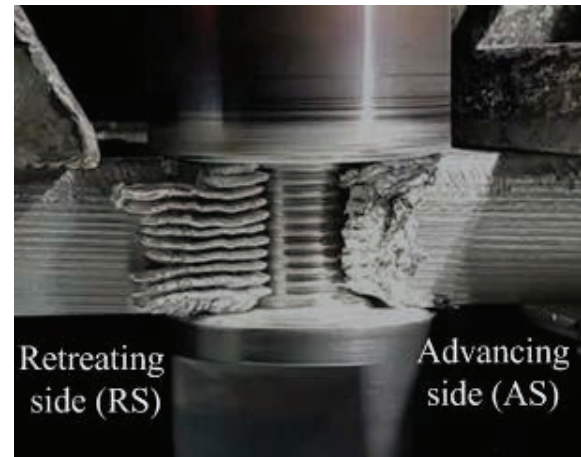
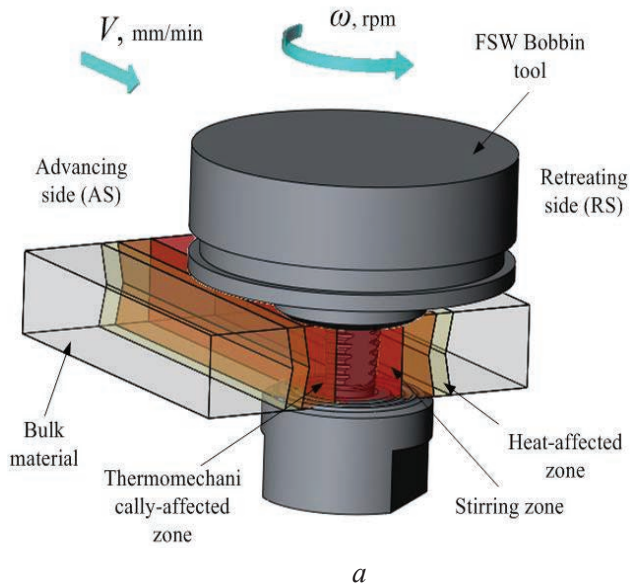


Fig. 1. Schematics (a) and the image (b) of the BFSW process with “bobbin tool” (c)

Table 1

Chemical composition of AA2024 alloy

Fe	Si	Mn	Ti	Cu	Mg	Zn	Others	Al
≤0,5	≤0,5	0,3-0,9	≤0,15	1,4-2,0	1,2-1,8	≤0,25	≤0,15	The rest

in Fig. 2), in the boundary sub-shoulder zone of the joint, and between the effect zones of the pin and the shoulder of the welding tool (BDR in Fig. 2), were selected for the study. Several cross sections of the welded joint were also studied (TD 1...3 in Fig. 2). For macro- and microstructure analysis, the samples were mechanically ground and polished, followed by chemical etching with Keller’s reagent (2 ml HF, 3 ml HCl, 5 ml HNO₃, and 190 ml H₂O) and examined with the Altami MET-1C optical microscope. Grain sizes were determined by the random secant line method. Microhardness measurements were performed according to GOST 9450-76 using the Duramin 5 hardness tester at a load of 50 gs. A four-sided diamond pyramid was used as an indenter. The data obtained were processed and visualized using the software package Origin.

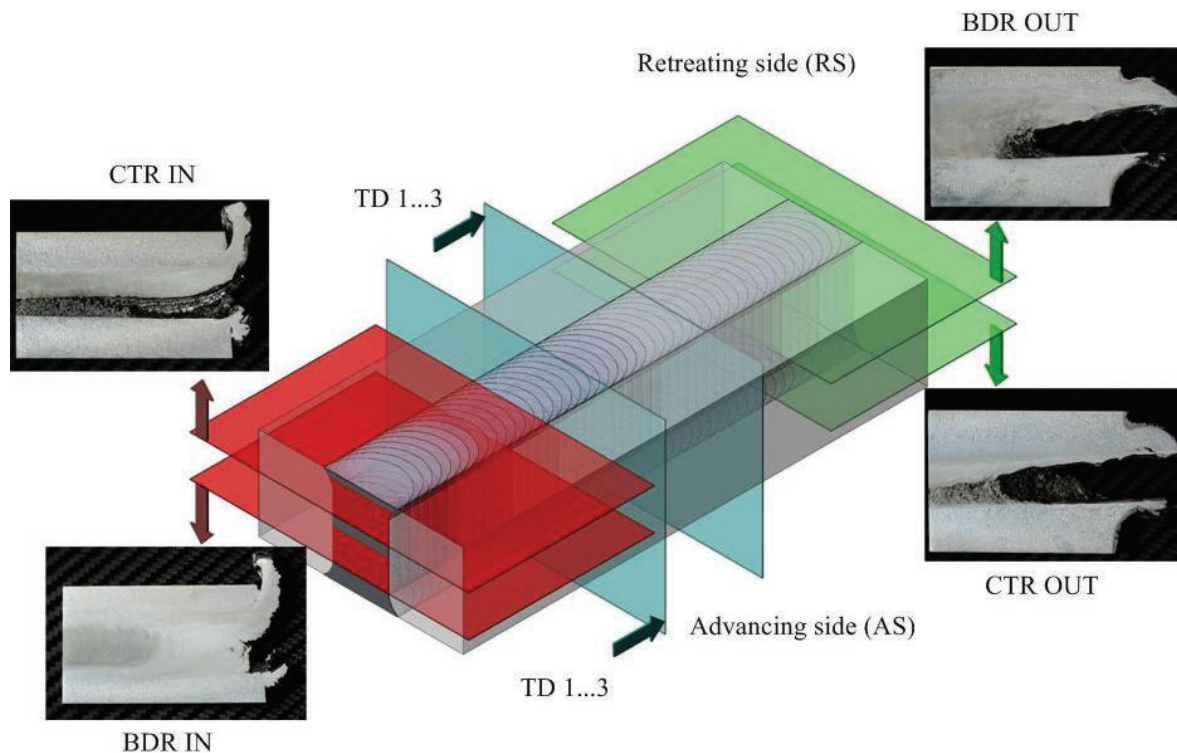


Fig. 2. Cutting scheme for investigation of a joint's structure: CTR/BDR longitudinal section of central/sub-shoulder zone; IN/OUT – initial/outgoing section; TD – transversely-directed cross-section

Results and Discussion

The tool inlet area at the starting point of a permanent joint is shown in Fig. 3, *a*. Under normal conditions, when the tool pin is fully plunged into the material, the plasticized metal is continuously transferred from the advancing side (AS) to the retreating side (RS) in front of the pin, and back behind it [20]. This is because the volume of plasticized metal is limited by the shoulder part of the tool and the unheated metal of the workpiece, as a result of which there is a directed adhesion-initiated extrusion of material from the retreating side into the area behind the tool. When the tool penetrates the material to be welded, the space behind the pin is not limited by the workpiece metal, so there is an intensive non-directional extrusion of the plasticized metal from the retreating side. It is caused by the contact of the material with the rotating tool, the cohesive interaction between the initial material and the plasticized material, and the intensive transfer of the plasticized material from the advancing side to the retreating side in the front of the tool. As a result, an area of extruded material is formed on the retreating side with a surface shape corresponding to the tool pin profile and traces of the extrusion process (1 in Fig. 3, *a*, *b*). By its nature, this process has common features with the extrusion of material from the friction zone during a dry or adhesion friction test with the formation of a metal overlap. For this reason, the friction stir processing or friction stir welding process can be represented as a dynamic extrusion of material along the retreating side, initiated by an adhesive frictional contact, from the front of the tool to the area behind the tool. At the same time, the welding process also requires a fragmented layer in front of the tool [22] that is capable of flowing around the tool pin without a direct grip and the formation of material breaks or cutting effects.

Moreover, the “RS – AS” transfer behind the tool is characterized by a much smaller volume of the transferred material, because it is based only on the adhesive interaction of the material with the tool. Under these conditions, the transferred material also undergoes an initial extrusion and adhesive contact with the formation of an irregularly shaped area of adhered metal on the advancing side (2 in Fig. 3, *a*, *b*). These processes result in the depletion of the welded joint with the material on the advancing side, which leads to the formation of an extended macro defect in the structure as a channel-type one (3 in Fig. 3, *a*, *b*). Further,

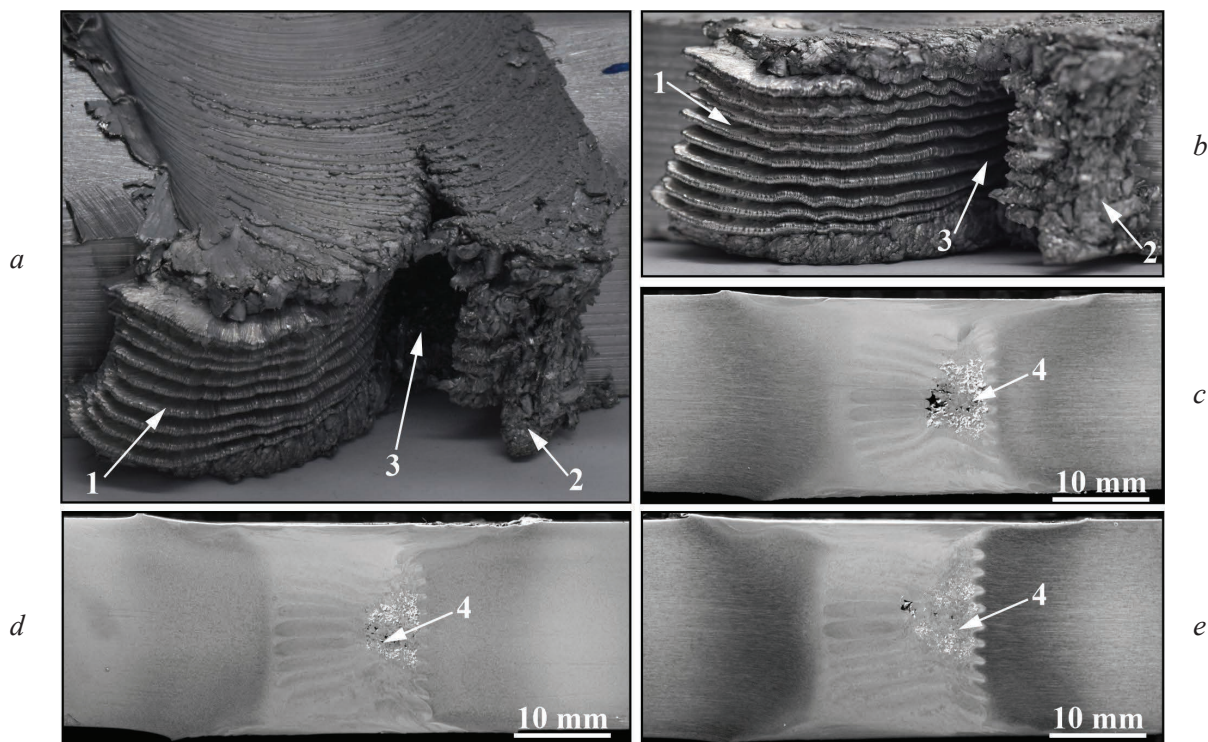


Fig. 3. Tool entry zone at the beginning of joint:

a, b – general view, *c, d, e* – cross-sectional views in region of 30–40 mm/min welding speed; 1 – region of upset metal with a complex shape; 2 – region of adhered metal with an irregular shape; 3 – channel-type defect; 4 – discontinuity flaws at channel extension zone

defects in the joint structure can be formed as discontinuities with a localization in the area of the initial channel formation at the tool inlet (4 in fig. 3, *c, d, e*). These defects are also associated with insufficient material densification in the welding zone, which causes the material extrusion and the formation of pores and discontinuities.

In the tool inlet zone, the material overlap formed on the retreating side (1 in Fig. 4, *a, d*) has a complex shape. As will be shown below, the metal structure in the overlapping zone is similar to the metal structure of the stir zone and, partially, the thermomechanically affected zone. The material adhered from the advancing side (2 in Fig. 4, *a, d*) also has a structure similar to that of the stir zone, but, due to the different formation nature, it is smaller than that from the retreating side. As the tool continues to move along the butt line, the material extruded from the retreating side partially occludes to form the highly defective structure of the stir zone (3 in Fig. 4, *a, d*). In the sub-shoulder zone, because of the larger amount of material involved in the process and the more limited formation zone, the “occlusion” of the material occurs much earlier than in the central part of the joint. At the initial stages, the volume of plasticized material is clearly visible in the boundary and central areas of the joint, which is caused by significant specific heat input from the tool rotation due to the low speed of its movement (4 in Fig. 4, *a, c*).

With a gradual increase in the movement speed to values of 20 mm/min and above, the specific heat input decreases. That leads to a decrease in the amount of plasticized metal and a decrease in the thermomechanically affected zone. Also, with the further tool movement, gradual densification of the material behind the tool and defect reduction is observed. This situation is caused by the intensification of the material extrusion process (Fig. 4, *a, d*). According to the literature data [21], the lower the rotation and tool movement speed ratio in a certain value range, the more effective is the transfer mechanisms between the retreating and advancing sides of the joint. In Fig. 4, *a, c, d*, it is seen that as the tool travel speed increases, the material amount on the advancing side of the joint increases, and a stir zone with a denser and less defective structure is formed (5 in Fig. 4, *a, d*). Closer to the tool outlet zone (Fig. 4, *b, e*) there is deconsolidation of the stir zone with the formation of a more defective structure (6 in Fig. 4, *b, e*) with

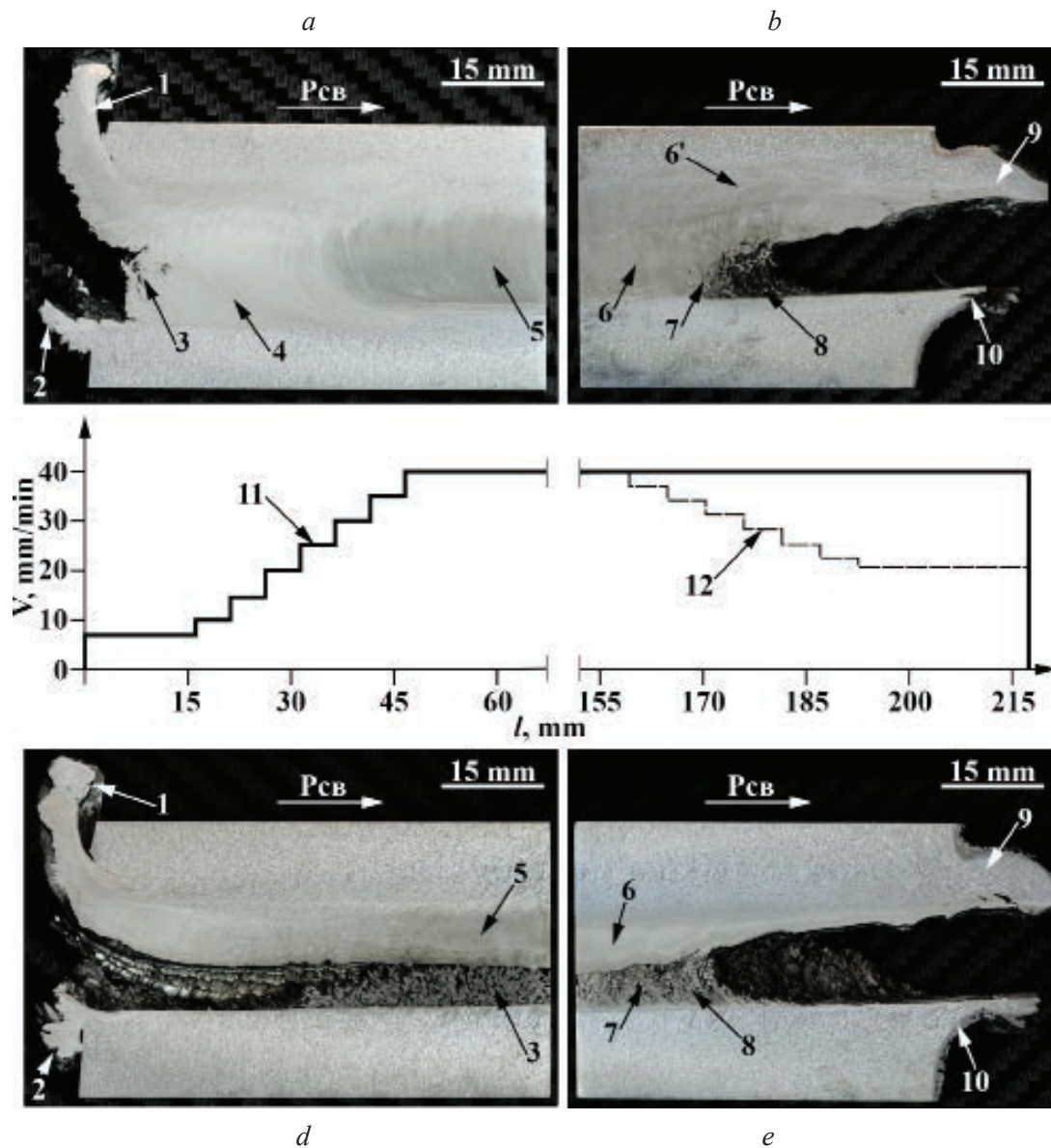


Fig 4. Joint formation at tool entry zone and joint failure at tool exit zone. Metallographic specimens at longitudinal sections of the joint:

a, b – sub-shoulder zone; *d, e* – central zone; *a, d* – tool inlet area; *b, e* – tool outlet area; *c* – variation of tool travel speed; 1, 2 – an overlap at retreating side and advancing side in tool inlet zone; 9, 10 – an overlap at retreating side and advancing side in the tool outlet area; 3 – joint packing region at tool inlet area; 4 – region of plasticized metal at tool inlet area; 5 – the stir zone at the tool inlet area, 6 – the stir zone before the joint failure at the tool outlet area; 7 – softened zone at the tool outlet area; 8 – zone of discontinuous structure; 11 – the curve of the tool travel speed variation 12 – the tool travel speed curve supposed to provide low structure imperfection at the tool outlet area

separation of two or more parts (6' in Fig. 4, b, e). Then the number of defects increases (7 in Fig. 4, b, e), and a channel-type defect is formed (8 in Fig. 4, b, e). Immediately at the tool outlet, large (9 in Fig. 4, b, e), and small material extrusion zones are formed (10 in Fig. 4, b, e), which are represented by significantly deformed material unlike the area of the tool inlet.

The length of the material extrusion zones at the tool outlet is determined by the welding speed, besides the physical nature of the process (11 in Fig. 4, c). During the tool inlet process, a gradual increase in the welding speed reduces defect formation and accelerates the joint formation process. But in the tool outlet area, a high welding speed, presumably, leads to a decrease in the fragmented material layer in the tool's front and a greater deformation effect on the material in front of this layer.

In turn, this process leads to the outstripping destruction of the joint structure in the tool outlet area. It is possible to reduce the defectiveness of the structure at the end of the joint, presumably, by an increase in the local heat and deformation influence on the material (to increase the fragmentation degree) by reducing the welding speed (12 in Fig. 4, c).

Differences in the stir zone formation at the tool inlet and outlet areas were investigated using optical microscopy (Fig. 5). Boundaries of the stir zone on the advancing side of the joint are more clearly

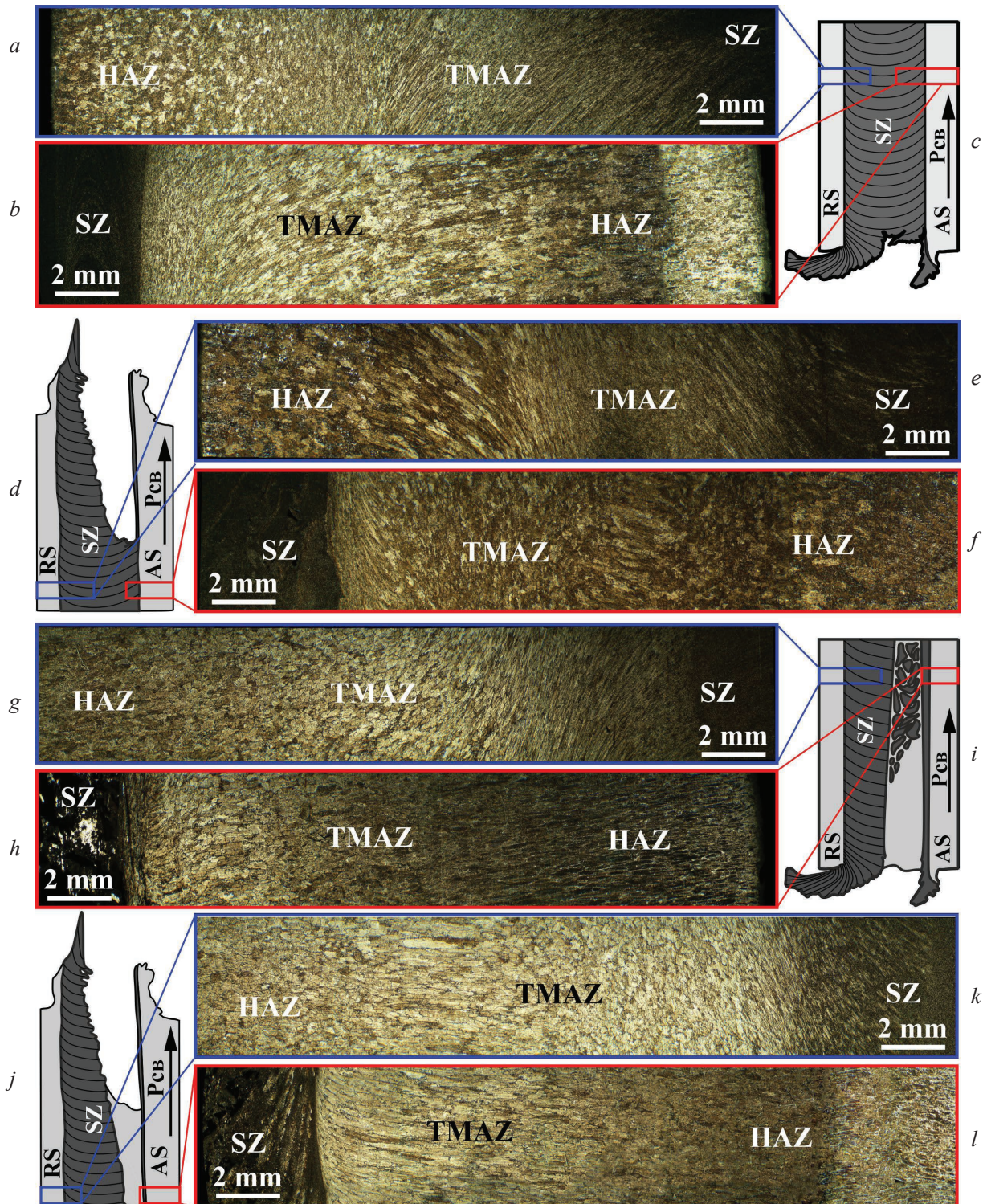


Fig. 5. Structure formation at joint obtained by BFSW:

a, b, e, i, g, h, k, l—structure in the stir zone (SZ) and thermomechanically affected zone (TMAZ) of sub-shoulder region (*a, b, e, f*) and central region (*g, h, k, l*) at advancing (*b, f, k, l*) and retreating (*a, e, g, k*) side of the joint; *c, d, i, j* — schematics of studied structures

distinguished (Fig. 5, *b, f, h, l*) than on the retreating side (Fig. 5, *a, e, g, k*). This can be explained by differences in the local thermomechanical processes. The material of the advancing side of the joint is less exposed to a temperature and deformation influence, as at welding there is a primary deformation of only a small part of it. On the retreating side, besides a similar deformation process, almost the entire volume of the plasticized material is extruded. For this reason, there is a sharper structural gradient in the retreating side region in the direction from the base metal to the stir zone. In the area of the structural gradient at the inlet (Fig. 5, *h*) and at the outlet (Fig. 5, *j*) of the tool, defects are observed as discontinuities in the stir zone.

In the shoulder effect zone of the welded joint (Fig. 5, *a-f*), the size of the main structural zones is significantly higher than in the tool pin effect zone (Fig. 5, *g-l*). The material of the main structural zones in the sub-shoulder area is characterized by less defectiveness, which is caused by the process of “clamping” behind the tool of the material extruded from the friction interaction area.

Besides the smaller size of the main structural zones, a sharper gradient in the structure of the thermomechanically affected zone can be observed on the advancing side compared to the structure of the retreating side (TMAZ in Fig. 5). A thin zone of thermomechanical influence is observed in the tool inlet and outlet areas. (Fig. 5, *h, j*). The material of the heat-affected zone is clearly distinguished from the base metal area in most images, which is due to its increased etchability (e.g., HAZ in Fig. 5, *b, j*). The typical structure of the main structural zones of the joint produced by the BFSW is shown in Fig. 6.

The base metal zone in this section is represented mainly by large equiaxed grains (Fig. 6, *a*). The average grain size in the base metal zone and the heat-affected zone is 40–45 μm . The material in the thermomechanically affected zone is represented by grains elongated and strongly deformed towards the

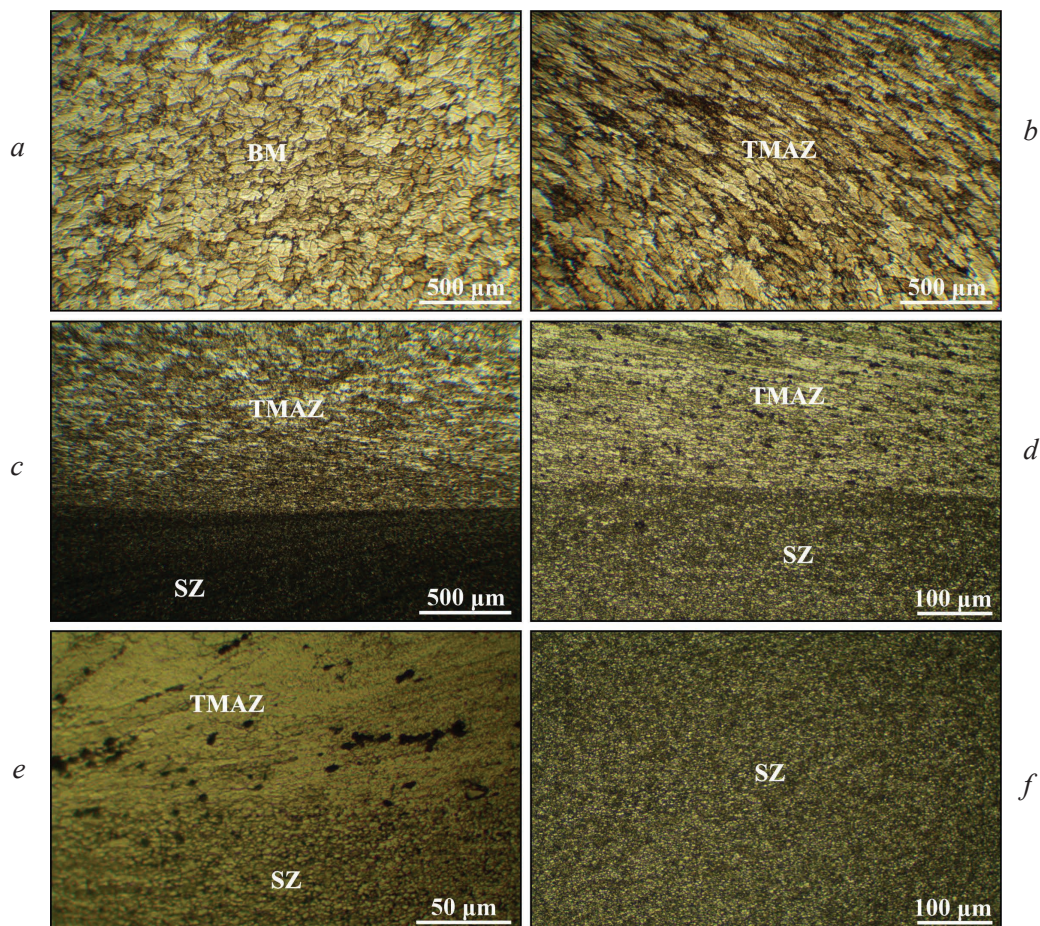


Fig. 6. Characteristic zones in the structure of the BFSW-joint:

a – base metal, *b* – thermomechanically affected zone, *c, d, e* – boundary between thermomechanically affected zone and stir zone, *f* – stir zone

metal flow direction (Fig. 6, b-d). In the thermomechanically affected zone near the stir zone, the grain size decreases from 40–45 μm to 2–3 μm . The average grain size in TMAZ is 40.9 μm .

The boundary between the stir zone and the thermomechanically affected zone is mostly smooth (Fig. 6, c-e), but differs for the advancing and retreating sides. When approaching from the thermomechanically affected zone to the stir zone, the refinement of large inclusions of secondary phases is observed (Fig. 6, e). There are no large inclusions detected in the stir zone. The structure of the stir zone (Fig. 6, f) is represented by finely dispersed equiaxed grains with an average size of 2.7 μm .

In the structure of BFSW-joints, defects of various types and structural-scale levels can be formed (Fig. 7). The defects can be caused by an asymmetry in the material stirring process, violation of the adhesive contact, imbalance in welding and tool rotation speeds, insufficient material densification in the welding zone, etc. At the boundary of the stir zone and the thermomechanically affected zone, discontinuities of different geometries can be observed (2 in Fig. 7).

Similar defects are formed in the stir zone together with defects like inhomogeneities in the grain structure (3 in Fig. 7). In some areas of the stir zone, defects as discontinuities are formed along the grain boundaries (4 in Fig. 7). The most critical defect in the structure is a defect in the form of a channel on the advancing side of the joint, which can be partially filled with the material of the stir zone (6 in Fig. 7). Such defects are formed because plasticized material enters the area behind the tool on the advancing side lastly. In combination with the continuous tool travel in the welding direction and the presence of existing discontinuities in the material, there is a constant shortage of the plasticized metal in this area.

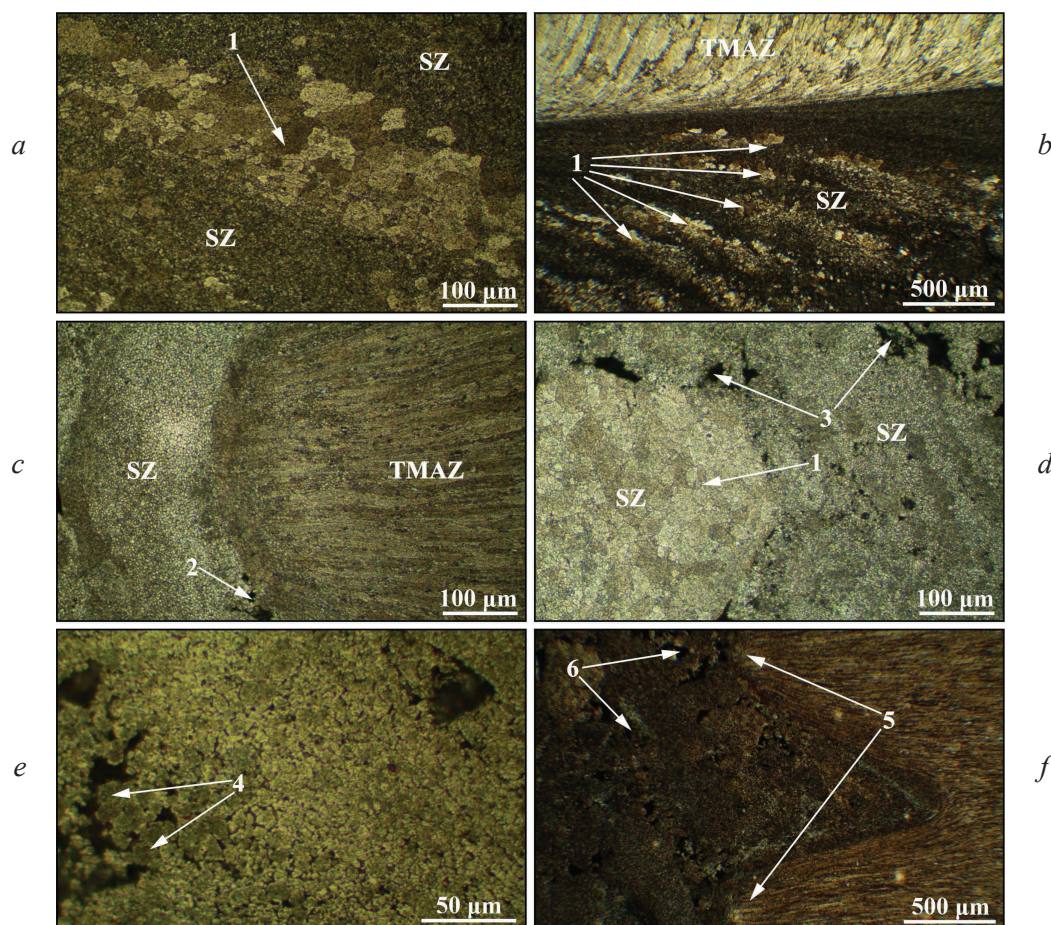


Fig. 7. Common structural defects of the BFSW-joint:

a, b – the inhomogeneity in the stir zone grain structure; *c-f* – discontinuities and pores at the stir zone and its boundary with the thermomechanically affected zone, *1* – the grain structure inhomogeneity; *2* – discontinuities at the boundary of the stir zone; *3, 4, 6* – discontinuities in the stir zone structure; *5* – the deformation heterogeneity at the advancing side of the joint

Thereby, the formation of a large-sized channel-type defect in the stir zone on the advancing side indicates a significant deviation of welding mode parameters, and the presence of a void filled with the material with a high content of structural discontinuities indicates an understatement of mode parameters. As a result, the formation of structural defects has a constant character and is accompanied by the formation of the thermomechanically affected zone, which repeats the contour of the tool pin with non-uniform deformation of the material (5 in Fig. 7).

Fig. 8, *a, b* shows the stir zone of the welded joint section with pronounced structural defects. The above features of the structure formation lead to the formation of a zone of structural discontinuities (1 in Fig. 8), which can be divided into two parts and contain large pores (1, 1' and 5 in Fig. 8). The metal flows along the tool contour in the area between the defect and the retreating side (I, II, II', II'' in Fig. 8) form a non-uniform structure with a "helical structure", consisting of zones with a different material deformation direction, which merge with each other.

However, the weld area without pronounced structural defects is significantly different (Fig. 8, *d*). In the joint structure, metal flows (I-IV in Fig. 8) reproduce the contour of the tool and form a system of parallel zones of material deformation. On the advancing side of the joint, the boundary of the stir and thermomechanically affected zones also repeats the shape of the tool (2 in Fig. 8). On the retreating side, the shape of the boundary is close to a straight line (3 in Fig. 8). At optimal parameters of the CFSW process in the welded joint formation of a monolithic core with the structure, in the literature called "onion rings" (concentric and similar in shape areas of deformed material) occurs, otherwise, formation of separate disconnected metal flows occurs [23]. Areas formed by individual metal flows can be observed clearly, and areas with "onion rings" features can be distinguished in each of them (Fig. 8, *e*). This structure indicates that at each metal flow a process occurs, which is similar to the processes occurring in the stir zone at the CFSW. As noted earlier, the joint formation is accompanied by the extrusion of the fragmented material on its retreating side from the area in front of the tool to the area behind the tool. If the pressure exerted by the extruded material on the material behind the tool determines the structure formation process, its greatest influence will be in the area where the temperature at the time of the local material transfer process is the maximum, that is, in the center of the flow (since the heat dissipation conditions in the center are significantly more difficult than at the edges). As a result, at each stage, the local metal flow will have a shape close to a dome. In this case, in the cross-section, the resulting structure will have the form of concentric rings of irregular shape in separate metal flows (Fig. 8, *d, e*).

These features of the stir zone structure cannot be explained exclusively by the adhesive interaction between the tool and the welded material, which is currently accepted as the main mechanism of the structure formation in friction stir welding [23]. One of the possible ways of such structure formation is the stepwise extrusive formation of the stir zone, which is consistent with the data of structural studies. The material extrusion manifests itself already at the initial stage of joint formation (Figs. 3–5). The extruded material structures at the tool inlet and the joint material are practically identical, with the presence of fine grains and a gradient transition to the base metal through the thermomechanically affected zone (Fig. 5). Presumably, the joint formation is accompanied by a grain size refinement to values conducive to deformation by the grain sliding [24] followed by a superplastic material flow of an extrusive nature. This makes friction stir welding and friction stir processing (FSP) similar to the superplastic deformation process, which is performed under conditions of a grain size refinement in the material to 1-10 μm at the appropriate temperature [25]. Consequently, the data obtained indicate the dual physical nature of the stir zone structure formation based on the adhesive transfer and extrusion of the material from the tool front area to the tool rear area.

The data on microhardness and grain size of the welded joint characteristic zones in its cross-section were compared (Fig. 9). The average value of microhardness in the stir zone equals $HV_{SZ} = 1.43$ GPa, in the heat-affected zone it equals $HV_{HAZ} = 1.17$ GPa, and in the thermomechanically affected zone, it equals $HV_{TMAZ} = 1.21$ GPa. The minimum values of microhardness correspond to a heat-affected zone that is caused by overaging of the material after the welding and by a weakening of a solid solution of the base metal. The hardness on the advancing side is more than on the retreating side, which is connected with the above-mentioned differences of thermomechanical processes on the corresponding sides and, consequently,

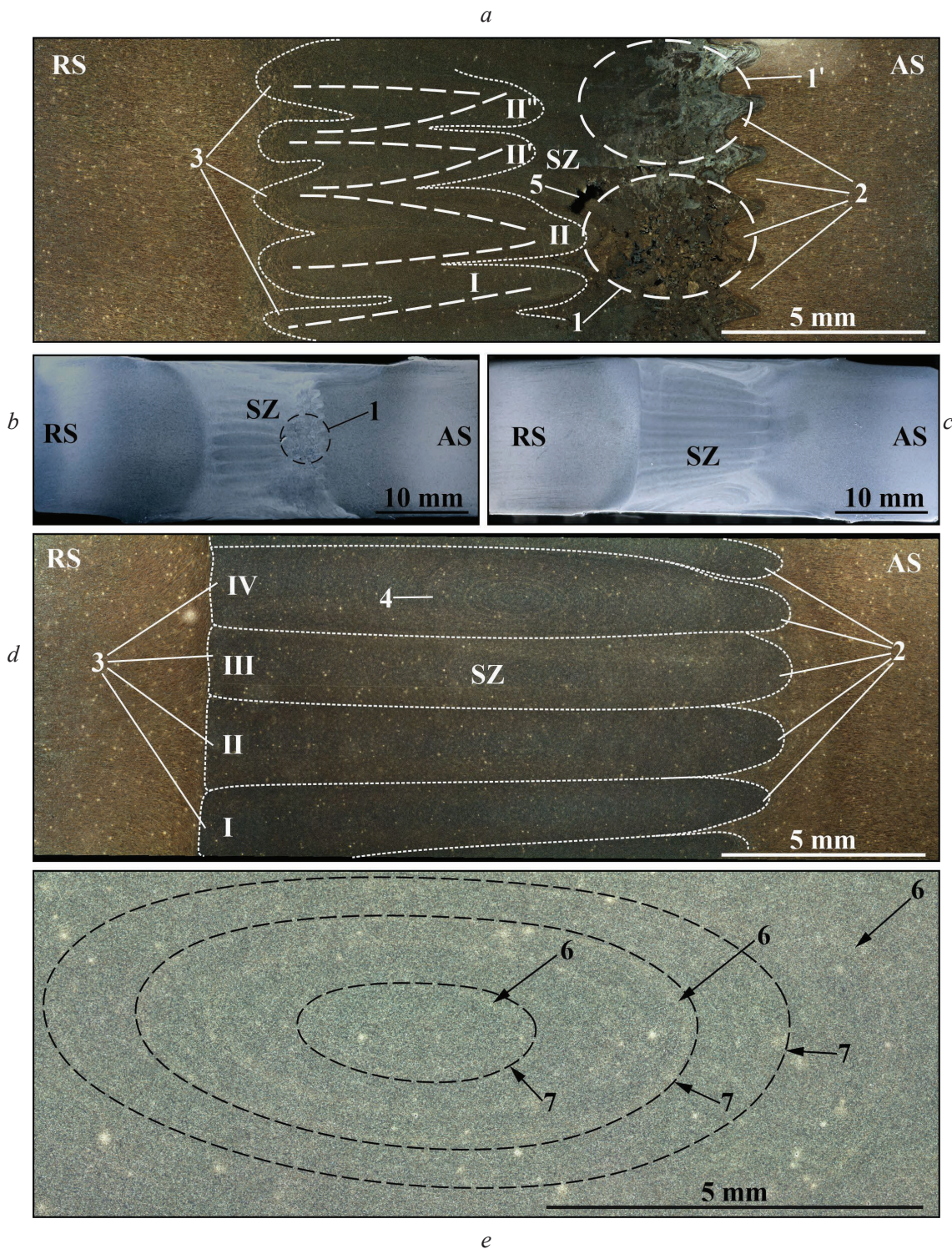


Fig. 8. Formation of metal flows around the tool:

a, b – at defective zone; *c, d, e* – at non-defective zone; 1 – channel-type defect; 2 – spikes formed with the welding tool's pin; 3 – metal flows at the stir zone; 4 – region of the “onion rings” structure formation from the metal flow; 5 – large imperfections at the stir zone; 6 – “onion rings” in the metal flow's structure; 7 – “onion rings” lines

the hardness on the advancing side of the joint is greater than on the retreating side, which is due to the above-mentioned differences in thermomechanical processes on the respective sides and, consequently, the different temperature effects on the material. The average base metal grain size is between 40–45 μm , in the thermomechanically affected zone it is 40.9 μm , and in the stir zone, it is 2.7 μm . The reduction of the grain size in the stir zone has a favorable effect on the mechanical properties, based on the Hall-Petch bar-

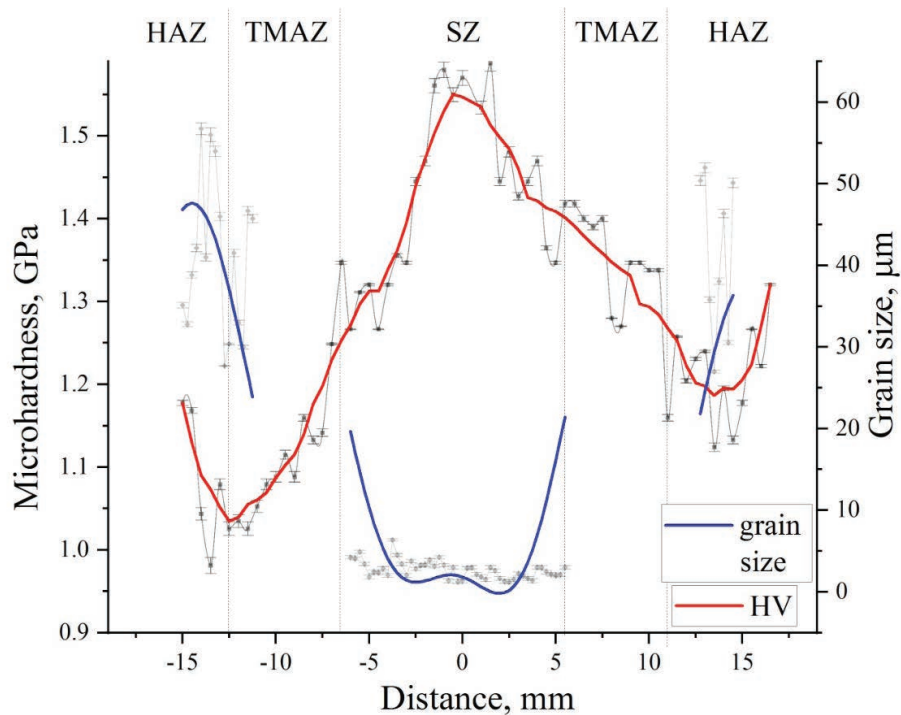


Fig. 9. Distribution of microhardness and grain size across the width of cross-sectional sample of the joint

rier effect. But the most significant strengthening effect, in this case, maybe the formation of a supersaturated solid solution due to the dissolution of secondary phase particles and the enrichment of the aluminum matrix with alloying elements [10]. This is confirmed by the scattering of measured microhardness values, which exceed the error ranges due to the indenter hitting the particles of secondary phases.

Conclusions

Conditions of the welded joint formation in the BFSW process are determined by the heat input into the welded material, its fragmentation, and plastic flow along the tool contour, which depend on the ratio between the rotation and travel speeds of the welding tool. The adjacent mechanisms of the joint formation are based on the combination of equally important processes of the adhesive interaction in the “tool-material” system and the metal extrusion into the area behind the welding tool. In combination with heat dissipation conditions and the configuration of the “tool-material” system, this leads to the extrusion of material from the welded joint and its deconsolidation. As a result, extended defects are formed, with the characteristic defect forming at the end of the welded joint regardless of the welding mode. The increase in the tool travel speed allows the specific heat input to be reduced. However, during welding of long joints, the amount of heat released in the joint increases due to the characteristic heat dissipation conditions. All this leads to a change in the conditions of adhesive interaction and extrusion processes, which leads either to the growth of already existing defects or to the formation of new ones. Taking into account the complexity of mechanisms of welded joint structure formation by the BFSW method, the defect-free welded joint production supposes mandatory use of various non-destructive control methods in combination with adaptive regulation of technological parameters directly in the welding process.

References

1. Threadgill P.L., Ahmed M.M.Z., Martin J.P., Perrett J.G., Wynne B.P. The use of bobbin tools for friction stir welding of aluminium alloys. *Materials Science Forum*, 2010, vol. 638–642, pp. 1179–1184. DOI: 10.4028/www.scientific.net/MSF.638-642.1179.



2. Fuse K., Badheka V. Bobbin tool friction stir welding: a review. *Science and Technology of Welding and Joining*, 2019, vol. 24 (4), pp. 277–304. DOI: 10.1080/13621718.2018.1553655.
3. Imam M., Sun Y., Fujii H., Ma N., Tsutsumi S., Murakawa H. Microstructural characteristics and mechanical properties of friction stir welded thick 5083 aluminum alloy. *Metallurgical and Materials Transactions A*, 2017, vol. 48, pp. 208–229. DOI: 10.1007/s11661-016-3819-6.
4. Liu X.M., Yao J.S., Cai Y., Meng H., Zou Z.D. Simulation on the temperature field of bobbin tool friction stir welding of AA 2014 aluminium alloy. *Applied Mechanics and Materials*, 2013, vol. 433–435, pp. 2091–2095. DOI: 10.4028/www.scientific.net/AMM.433-435.2091.
5. Yang C., Ni D.R., Xue P., Xiao B.L., Wang W., Wang K.S., Ma Z.Y. A comparative research on bobbin tool and conventional friction stir welding of Al-Mg-Si alloy plates. *Materials Characterization*, 2018, vol. 145, pp. 20–28. DOI: 10.1016/j.matchar.2018.08.027.
6. Esmaily M., Mortazavi N., Osikowicz W., Hindsefelt H., Svensson J.E., Halvarsson M., Martin J., Johansson L.G. Bobbin and conventional friction stir welding of thick extruded AA6005-T6 profiles. *Materials and Design*, 2016, vol. 108, pp. 114–125. DOI: 10.1016/j.matdes.2016.06.089.
7. Goebel J., Reimann M., Norma A., Dos Santos J.F. Semi-stationary shoulder bobbin tool friction stir welding of AA2198-T851. *Journal of Materials Processing Technology*, 2017, vol. 245, pp. 37–45. DOI: 10.1016/j.jmatprotec.2017.02.011.
8. Xu W., Luo Y., Zhang W., Fu M. Comparative study on local and global mechanical properties of bobbin tool and conventional friction stir welded 7085-T7452 aluminum thick plate. *Journal of Materials Science and Technology*, 2018, vol. 34, pp. 173–184. DOI: 10.1016/j.jmst.2017.05.015.
9. Milčić M., Burzić Z., Radisavljević I., Vuherer T., Milčić D., Grabulov V. Experimental investigation of fatigue properties of FSW in AA2024-T351. *Procedia Structural Integrity*, 2018, vol. 13, pp. 1977–1984. DOI: 10.1016/j.prostr.2018.12.220.
10. Eliseev A.A., Kalashnikova T.A., Gurianov D.A., Rubtsov V.E., Ivanov A.N., Kolubaev E.A. Ultrasonic assisted second phase transformations under severe plastic deformation in friction stir welding of AA2024. *Materials Today Communications*, 2019, vol. 21, p. 100660. DOI: 10.1016/j.mtcomm.2019.100660.
11. Dong J., Gao C., Lu Y., Han J., Jiao X., Zhu Z. Microstructural characteristics and mechanical properties of bobbin-tool friction stir welded 2024-T3 aluminum alloy. *International Journal of Minerals, Metallurgy, and Materials*, 2017, vol. 24, pp. 171–178. DOI: 10.1007/s12613-017-1392-7.
12. Ivanov A.N., Rubtsov V.E., Kolubaev E.A., Bakshaev V.A., Ivashkin I.N. Vliyanie rezhima svarki treniem s peremeshivaniem i ee napravleniya odnositel'no napravleniya prokatki splava D16 na strukturu i svoystva ego svarykh soedinenii [Effect of friction stir welding mode and its direction relative to the rolling direction of 2024 alloy on the structure and mechanical properties of its weld joints]. *Obrabotka metallov (tehnologiya, oborudovanie, instrumenty) = Metal Working and Material Science*, 2020, vol. 22, no. 4, pp. 110–123. DOI: 10.17212/1994-6309-2020-22.4-110-123.
13. Li G.H., Zhou L., Luo S.F., Dong F.B., Guo N. Quality improvement of bobbin tool friction stir welds in Mg-Zn-Zr alloy by adjusting tool geometry. *Journal of Materials Processing Technology*, 2020, vol. 282, p. 116685. DOI: 10.1016/j.jmatprotec.2020.116685.
14. Wu D., Li W.Y., Gao Y.J., Yang J., Su Y., Wen Q., Vairis A. Effect of an improved pin design on weld formability and mechanical properties of adjustable-gap bobbin-tool friction stir welded Al-Cu aluminum alloy joints. *Journal of Manufacturing Processes*, 2020, vol. 58, pp. 1182–1188. DOI: 10.1016/j.jmapro.2020.09.015.
15. Zhang H., Wang M., Zhang X., Yang G. Microstructural characteristics and mechanical properties of bobbin tool friction stir welded 2A14-T6 aluminum. *Materials and Design*, 2015, vol. 65, pp. 559–566. DOI: 10.1016/j.matdes.2014.09.068.
16. Li G., Zhou L., Zhang J., Luo S., Guo N. Macrostructure, microstructure and mechanical properties of bobbin tool friction stir welded ZK60 Mg alloy joints. *Journal of Materials Research and Technology*, 2020, vol. 9, iss. 4, pp. 9348–9361. DOI: 10.1016/j.jmrt.2020.05.067.
17. Chen S., Li H., Lu S., Ni R., Dong J. Temperature measurement and control of bobbin tool friction stir welding. *The International Journal of Advanced Manufacturing Technology*, 2016, vol. 86, pp. 337–346. DOI: 10.1007/s00170-015-8116-9.
18. Tamadon A., Pons D.J., Clucas D. Structural anatomy of tunnel void defect in bobbin friction stir welding, elucidated by the analogue modelling. *Applied System Innovation*, 2020, vol. 3, p. 2. DOI: 10.3390/asi3010002.
19. Tamadon A., Pons D.J., Clucas D., Sued K. Internal material flow layers in AA6082-T6 butt-joints during bobbin friction stir welding. *Metals*, 2019, vol. 9, p. 1059. DOI: 10.3390/met9101059.



20. Seidel T.U., Reynolds A.P. Visualization of the material flow in AA2195 friction-stir welds using a marker insert technique. *Metallurgical and Materials Transactions A*, 2001, vol. 32, pp. 2879–2884. DOI: 10.1007/s11661-001-1038-1.
21. Zhu Z., Wang M., Zhang H., Zhang X., Yu T., Wu Z. A finite element model to simulate defect formation during friction stir welding. *Metals*, 2017, vol. 7, p. 256. DOI: 10.3390/met7070256.
22. Tamadon A., Pons D.J., Sued K., Clucas D. Formation mechanisms for entry and exit defects in bobbin friction stir welding. *Metals*, 2018, vol. 8, p. 33. DOI: 10.3390/met8010033.
23. Kalashnikova T., Chumaevskii A., Kalashnikov K., Fortuna S., Kolubaev E., Tarasov S. Microstructural analysis of friction stir butt welded Al-Mg-Sc-Zr alloy heavy gauge sheets. *Metals*, 2020, vol. 10 (6), p. 1–20. DOI: 10.3390/met10060806.
24. Kozlov E.V., Trishkina L.I., Popova N.A., Koneva N.A. Dislocation physics in the multilevel approach to plastic deformation. *Physical Mesomechanics*, 2011, vol. 14, p. 283. DOI: 10.1016/j.physme.2011.12.007.
25. Grimes R. Superplastic forming of aluminium alloys. *Superplastic forming of advanced metallic materials: methods and applications*. Ed. by G. Giuliano. Cambridge, Philadelphia, PA, Woodhead Publishing, 2011, pp. 247–271.

Conflicts of Interest

The authors declare no conflict of interest.

© 2021 The Authors. Published by Novosibirsk State Technical University. This is an open access article under the CC BY license (<http://creativecommons.org/licenses/by/4.0/>).